buildings

MDPI

Article

Effective Flange Width Based on Equivalence of Slab Crack Width at Hogging Moment Region of Composite Frame Beam

Mu-Xuan Tao [1], Ze-Bin Zou [1] and Ji-Zhi Zhao [2,*]

[1] Department of Civil Engineering, Tsinghua University, Beijing 100084, China; taomuxuan@tsinghua.edu.cn (M.-X.T.)
[2] School of Civil Engineering, Chongqing University, Chongqing 400045, China
* Correspondence: 13120084917@163.com

Abstract: Steel–concrete composite structures have advantages in terms of strong bearing capacity and full utilisation of performance, and thus, composite frame beams are widely used in building construction. However, in the design and use of existing composite frame beams, the composite effect of a slab and steel beam cannot be completely taken into account. In this study, the effective flange width method is utilised to calculate the contribution of the slab reinforcement to the section moment of inertia to check the beam-end crack width via simulations using the general finite-element software MSC.MARC 2020. A parameter sensitivity analysis of the reinforcement tensile stress is conducted to determine critical influential geometric parameters for the side-column and centre-column hogging moment regions. Finally, design formulae for calculating the effective flange widths of the side- and centre-column hogging moment regions are proposed. In the formula for the side-column hogging moment region, the half column width (R) and steel-beam height (h_s) are critical variables, whereas, in the formula for the centre-column hogging moment region, the steel-beam height (h_s), slab width (b_c), and half clear-span length (l) are critical variables. Both formulas are verified via a multiparameter simulation, which enables more accurate crack-checking calculations for the hogging moment region in the serviceability limit state. This study provides an important reference for fine finite-element simulations of serviceability limit states and shows the factors affecting the effective flange width that differ from those in the ultimate limit state.

Keywords: steel–concrete composite structure; composite frame beam; hogging moment region; effective flange width; parameter sensitivity analysis

check for updates

Citation: Tao, M.-X.; Zou, Z.-B.; Zhao, J.-Z. Effective Flange Width Based on Equivalence of Slab Crack Width at Hogging Moment Region of Composite Frame Beam. *Buildings* **2024**, *14*, 1708. https://doi.org/10.3390/buildings14061708

Academic Editor: Hiroshi Tagawa

Received: 15 April 2024
Revised: 28 May 2024
Accepted: 5 June 2024
Published: 7 June 2024

Copyright: © 2024 by the authors. Licensee MDPI, Basel, Switzerland. This article is an open access article distributed under the terms and conditions of the Creative Commons Attribution (CC BY) license (https://creativecommons.org/licenses/by/4.0/).

1. Introduction

Composite frame beams (CFBs) fully utilise the compressive and tensile properties of concrete and steel, respectively, with the anchoring relationship between components and exhibit high bearing capacities, lateral stiffness, and material utilisation rates [1–5]. The composite effect between the slab and steel beam reduces the maximum bending moment in the positive bending moment region and increases the bearing capacity [6,7]. However, in the hogging moment region (HMR), owing to the anchoring effect of the bolts on the upper flange of the steel beam, the concrete slab will crack under tension; therefore, it is necessary to calculate and verify the crack width [8]. In a crack-width calculation method proposed in an earlier study, the composite effect of the reinforcement and steel beams is ignored, and the calculation results are conservative and do not reasonably account for the contribution of the reinforcement to the cracked composite section [9].

Several investigations have been conducted on the behaviour of CFBs in various aspects. Elkelish and Robinson [10] studied the effective flange widths (EFWs) of ribbed concrete–slab composite beams using the layered-design method and determined several to be influential parameters. Amadio and Fragiacomo [11] demonstrated that the EFW of a CFB under the rigid-connection hypothesis is greater than that under the deformed-connection hypothesis and that the existence of the shear lag effect makes it necessary

to calculate the EFW. Subsequently, a number of studies [12–15] have focused on the calculation of the EFWs of circular and square concrete-filled steel tube columns (CFSTs) and indicated that the existing EFW calculation method has a problem in terms of load mode mismatch, considers only the ultimate limit state of the bearing capacity, and is not suitable for crack-checking calculations.

In order to calculate the crack width more accurately, it is necessary to consider the spatial combination of the floor slabs, and the calculation of the EFW of the floor slab is a feasible and effective method. The sectional moment of inertia obtained in this way is not underestimated, so the value of the stresses in the reinforcement becomes smaller at the same value as the bending moment. In this situation, the calculated crack width is smaller and closer to the real result, which is critical for accurate corrosion prevention judgement [16]. Therefore, this study is based on research conducted thus far on the composition of CFBs and analyses the contribution of slab reinforcement to the sectional moment of inertia in the HMRs of CFBs in the serviceability limit state (SLS).

First, the software MSC.MARC 2020 is used to establish finite-element (FE) models that can simulate the stress distribution of the slab reinforcement of the side and centre columns.

Second, after the FE model is established, the EFW of the slab in the side and centre columns can be obtained via calculation. The geometric parameters of the CFSTs, steel beam, transom, and slab are used to conduct a sensitivity analysis of the EFW to obtain its influential parameters.

Third, multiple linear regression is conducted using these parameters to obtain formulae for the EFWs of the side and centre columns. In the process of formula verification, a large number of models generated by combinations of the influential parameters are involved in the error analysis.

The research and modelling methods used in this study have been verified in past research studies, relative to which several improvements and innovations have been made in this study, as follows:

First, the analysis of the composite effect in CFBs focuses mainly on SLS, which is consistent with the structural state corresponding to the crack-width checks in engineering construction.

Second, the FE model used in this study establishes and hypothesises on each part more accurately, with the MARC subroutine involving both the side and centre columns, to realise uniform loading using displacement controls. By contrast, past research studies typically adopted centralised loading.

Finally, the analysis of the parameters influential on the EFW is more comprehensive, and the relevant geometric parameters are modelled, calculated, and analysed in their entirety. The proposed formulas are convenient for use in engineering applications and have been verified to be of remarkable accuracy.

2. Finite-Element Models of Composite Frame Beams

In this section, the development of an accurate FE model is presented, in which shell elements, boundary conditions for uniform loads, and hinge joints are used. Simplified formulas for calculating the reinforcement laying width and EFW are proposed. The component modelling, parameter values, model loads, etc. are as follows:

2.1. Component Modelling and Parameter Values

The development of cracks at the end of a CFB with a uniform load and the calculation of the crack width are the primary focus of this study. To improve the utilisation of materials in engineering a CFB, it is necessary to conduct more precise simulations and calculations of the HMR. According to the studies on the ultimate limit state, a CFB is divided into four parts, i.e., CFSTs, steel beam, transom, and slab, which can be used to model the structure in FE software [12–15]. This study extends and improves on that earlier model and includes a double-span model for comparison.

The element types of the four components are selected, as shown in Table 1. The slab is simplified into layered shell elements based on the calculation efficiency of the model and stud elements on half of the connection between the plate and steel beam. The slab reinforcement layer is an important position for deriving and calculating the stress results. In the five-layered shell elements, the middle layer is set to be the reinforcement layer according to the reinforcement ratio, which is fixed at 1%, whereas the upper and lower layers are configured to be the concrete layer and concrete protective layer, respectively, as shown in Figure 1. The connection between the slab and the steel beam can be made in several methods during the actual modelling process, and in this study, the option of using rigid rod connections can improve the efficiency of the parametric modelling process without losing the accuracy of the results [17]. Under this condition, the slip effect is excluded, and rod elements are directly used to connect the layered shell and shell elements, as shown in Figure 2 [18]. As a comparison, the model method with slip effect is shown in Figure 3a used in Ref. [9], of which the numerical results are consistent with the test results in Ref. [10] as shown in Figure 3b–d. The difference between the two methods, excluding and including the slip effect, is not significant, so the slip effect is not considered [19–22].

Table 1. Component elements.

Components	Materials	Element Type Keywords
CFSTs	Concrete, Steel	Mech_three_shell, Mech_three_solid
Steel beams	Steel	Mech_three_shell
Transoms	Steel	Mech_three_shell
Floor	Concrete, Steel	Mech_three_shell, Mech_three_solid, Mech_three_beam_ela

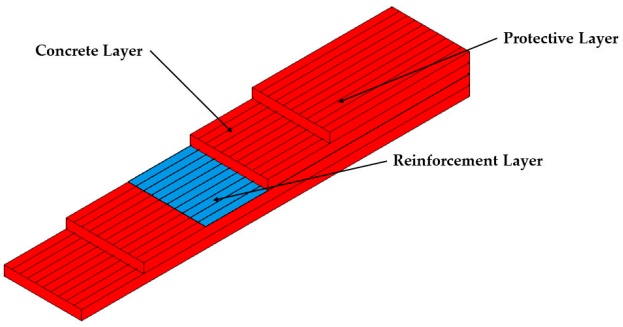

Figure 1. Layered shell elements of the slab.

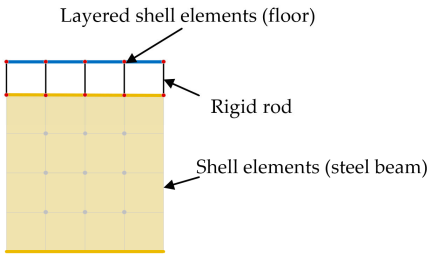

Figure 2. Connection between slabs and steel beams.

Figure 4 shows the modelling results of the single-span and double-span models, whereas Table 2 outlines the model geometry and material parameters of the other components with a fixed cell length of 50 mm. Because the study is on SLS, both the steel tubes and concrete of the CFSTs are assumed to be consistently in the elastic stage, whereas the concrete compression is assumed to follow a Rüsch curve, linear softening under tension,

and dispersion crack model [15,23]. Moreover, the slab reinforcement, steel beams, and cross beams are assumed to behave in accordance with ideal elastic–plastic models.

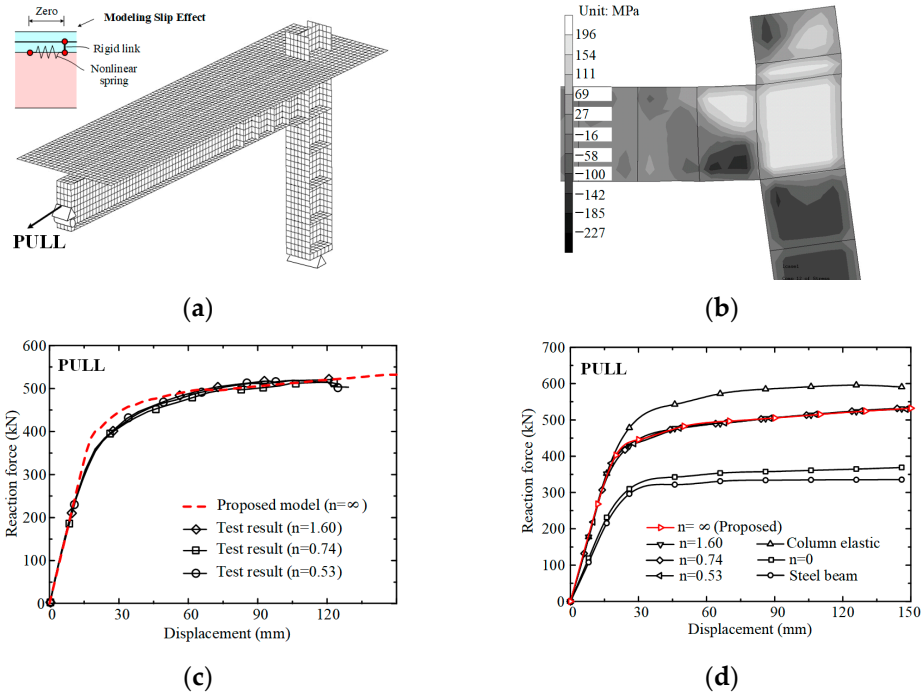

Figure 3. Simulation of the composite frames tested and analysed. (Reprinted with permission from Ref. [12] 2012, Nie et al.). (**a**) Elaborate FE model. (**b**) Shear stress at the positive displacement of 150 mm. (**c**) Comparison of test and numerical results. (**d**) Comparison of numerical results and with different parameters.

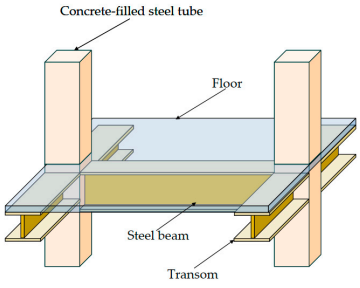

(**a**) Single-span model

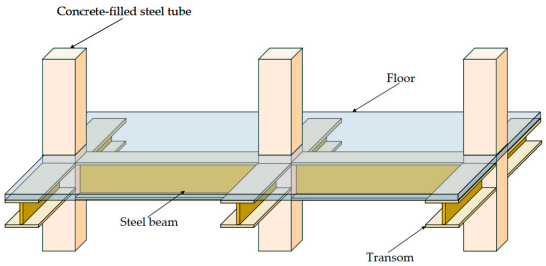

(**b**) Double-span model

Figure 4. Composite frame beam models.

Table 2. Parameters of four components.

Components	Secondary Components	Parameters
CFSTs	Concrete Steel tube	$H = 3000$ mm, $R = 200$ mm $t_{co} = 10$ mm
Steel beams	\	$bf_{top} = 200$ mm, $bf_{bottom} = 200$ mm, $h_s = 400$ mm, $t_f = 12$ mm, $t_w = 8$mm, $f_y = 350$ MPa
Transoms	\	$btr_{top} = 200$ mm, $btr_{bottom} = 200$ mm, $h_{tr} = 300$ mm, $t_{ftr} = 12$ mm, $t_{wtr} = 8$ mm, $f_{ytr} = 350$ MPa
Floor	Concrete Reinforcement	$h_c = 100$ mm, $b_c = 2000$ mm, $l = 3000$ mm $f_{yr} = 300$ MPa, $\rho = 1\%$

Note: H = 50% height of CFST; R = 50% width of CFST; t_{co} = thickness of steel tube; bf_{top} = width of top flange of steel beams; bf_{bottom} = width of bottom flange of steel beams; h_s = height of web of steel beams; t_f = thickness of flanges of steel beams; t_w = thickness of web of steel beams; f_y = yield stress of steel beams; btr_{top} = width of top flange of transoms; btr_{bottom} = width of bottom flange of transoms; h_{tr} = height of web of transoms; t_{ftr} = thickness of flanges of transoms; t_{wtr} = thickness of web of transoms; f_{ytr} = yield stress of transoms; h_c = height of slab; b_c = width of slab; l = 50% clear-span length of slab, equal to the length of the steel beams; f_{yr} = yield stress of slab reinforcement; ρ = reinforcement ratio.

2.2. Model Loading and Boundary Conditions

In earlier research studies, the ultimate limit state of the load capacity had been based mainly on single-point displacement control loading, which is not in line with the actual load of a CFB slab surface [15]. To perform accurate calculations on the cracking problem in the HMR, a uniform load will have to be applied to the slab surface. In the end, the uniform load is simplified to six equal points for each steel beam using displacement control. In the concrete realisation of the model, Uforms, a subroutine based on a MARC secondary development, is used.

The selection of boundary conditions for the model also has a great influence on the simulation results. The object of this study is a recurring basic unit in the whole of the composite frame structure, and the loading method is static. In other types of structures, such as bridge structures, springs of various stiffnesses are usually the appropriate boundary conditions, while in composite frame structures, CFST are bound to exist at the point where the bending moment value is zero, named the inflection point, which is set at the midpoint of the whole column in consideration of the symmetry [24]. The hinge joint is chosen as the boundary condition because it is necessary to relax the rotation constraints while providing displacement constraints at the inflection point [21]. The single-span model adds constraints at four positions above and below the two columns, whereas the double-span model adds constraints at six positions on the three columns. The boundary constraints of the models are shown in Figure 5.

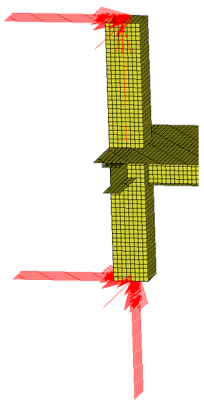

Figure 5. Boundary constraints in Marc models.

2.3. Serviceability Limit State Condition

This study focuses on checking the crack width of the HMR beam. However, the load value of SLS is typically low, and the judgement conditions are not uniform. According to earlier research results, methods for calibrating the limit state of the carrying capacity are accurate and efficient [15,23]. In the present study, the SLS state is based on the ultimate limit state, such that SLS is assumed to be the state wherein the load reaches 0.5 times the carrying capacity of the ultimate limit state [24,25]. This calculation method was used in previous experiments on composite beams to predict the prestressed tensile force of SLS, and the results were, in general, consistent with the experiments [26,27]. Its formula is as follows:

$$P = 0.5 \times P_{\mathrm{u}} \tag{1}$$

where P represents the loading force of SLS, and P_{u} denotes the load force of the ultimate limit state.

The criterion for judging the ultimate limit state of the carrying capacity is complex, and according to the literature, it is simplified to use the deflection of the centre point of the slab as the judging standard [25,26]. The specific centre deflection of the slab is set to reach 0.02 times the span of the slab as the ultimate limit state signal, and the calculation formula is as follows:

$$w_{\mathrm{c}} = 0.02 \times l \tag{2}$$

where w_{c} represents the deflection of the centre point on the slab, and l is the geometric parameter of the slab, which indicates the 50% clear-span length of the slab.

The EFW is calculated using the ratio of the reinforcement stress integral in the HMR to the maximum reinforcement stress. The formula is as follows:

$$b_{\mathrm{e}} = \int_{-\frac{b_{\mathrm{c}}}{2}}^{\frac{b_{\mathrm{c}}}{2}} \frac{\sigma}{\sigma_{\max}} \mathrm{d}x \tag{3}$$

where b_{e} represents the EFW, b_{c} is the slab width, and σ and $\sigma_{\max}$ denote the stress along the slab width and the maximum stress, respectively. In this formula, the reinforcement stress integral is equal to the area surrounding the stress curve. Changes in the area size or integral range of various geometric parameters can lead to an increase or decrease in the EFW.

3. Sensitivity Analysis of Influential Parameters

Once a precise FE model of the CFB has been established using a general FE software such as MARC 2020, the reinforcement stress in the HMR can be extracted and calculated, and the EFW can be obtained for analysis. Comparisons between the EFWs calculated for the single-span and double-span models can reveal the relationship between the two models. Subsequently, because the CFB is composed of four parts, i.e., CFST, steel beams, transoms, and slabs, sensitivity analysis is conducted on all geometric parameters of the four members to uncover the crucial parameters that influence the EFW of the HMR. As mentioned in Equation (3), the change in magnitude of EFW caused by geometric parameters is an important reference for sensitivity in determining the influential parameters.

3.1. Geometric Parameters of Model and Methods of Sensitivity Analysis

The main influential parameters discussed in this study, particularly in the construction of an FE model, are the geometric parameters of the four parts of the CFB. In the sensitivity analysis, several parameters within an appropriate selection range should be selected, as shown in Table 3. The relationship between the parameters and EFW can be obtained by analysing the model with different values for a single parameter.

Table 3. Geometric parameter values.

Components	Geometric Parameters (Standard Model Value)	Parameter Values (mm)	Value Range (Comparing the Standard Value)
CFST	$H = 3000$ mm	2000, 2500, 3000, 3500, 4000, 5000, 6000	−50% to +100%
	$R = 200$ mm	100, 150, 200, 250, 300, 350, 400, 450, 500, 550, 600	−50% to +200%
	$t_{co} = 10$ mm	6,8,10,12,14,16,18,20	−40% to +100%
Steel beams	$bf_{top} = 200$ mm	100, 200, 300, 400	−50% to +100%
	$bf_{bottom} = 200$ mm	100, 200, 300, 400	−50% to +100%
	$h_s = 400$ mm	200, 250, 300, 350, 400, 450, 500, 550, 600, 650, 700, 750, 800	−50% to +100%
	$t_f = 12$ mm	8, 10, 12, 14, 16, 20, 24	−50% to +100%
	$t_w = 8$ mm	6, 8, 10, 12, 14, 16	−25% to +100%
Transoms	$btr_{top} = 200$ mm	100, 200, 300, 400	−50% to +100%
	$btr_{bottom} = 200$ mm	100, 200, 300, 400	−50% to +100%
	$h_{tr} = 300$ mm	200, 250, 300, 350, 400, 450, 500, 550, 600, 650, 700, 750, 800	−50% to +167%
	$t_{ftr} = 12$ mm	8, 10, 12, 14, 16, 20, 24	−50% to +100%
	$t_{wtr} = 8$ mm	6, 8, 10, 12, 14, 16	−25% to +100%
Floor	$b_c = 2000$ mm	1400, 1700, 2000, 2300, 2600, 2900, 3200, 3500, 3800, 4100	−30% to +110%
	$l = 3000$ mm	2100, 2550, 3000, 3450, 3900, 4350, 4800, 5250, 5700	−30% to +90%

The material parameters, which are not the concern of this study, such as concrete compressive strength and yield stress of steel, are set at general values, e.g., C30 concrete, and the yield stress of steel reinforcement (f_{yr}) equal to 300 MPa. In this study, we expect to find out the influence of geometrical parameters on the distribution of stress in steel reinforcement, and the material parameters, although they also have a certain influence on EFW, will be discussed in future studies.

Criteria for parameter sensitivity analysis are used to identify parameters in the analysis that have a significant impact on EFW, which will provide a basis for fitting the EFW formula. There are various algorithms for parameter sensitivity analyses in existing studies, including methods that use sensitivity coefficients to evaluate and delineate sensitivity thresholds. Since, in this study, the geometrical parameters are individually divided and analysed, it is more straightforward to select the parameters using the division of the sensitivity threshold, which in this study is 15% [12,15,19,28].

3.2. EFW of Side Columns

3.2.1. Influential Parameters for Side Columns

Based on the analysis of EFWs in the single-span and double-span models, the influential parameters reflected by the two models are the same: the CFST half-width (R) and steel-beam height (h_s), as shown in Figure 6. In the two models, the relationship between the EFW and R for the HMR clearly exhibits a segmental linear correlation. When R is less than 300 mm, the EFW increases as R is increased, until R reaches 300 mm, beyond which the EFW no longer increases. By contrast, the EFW decreases significantly as h_s is increased.

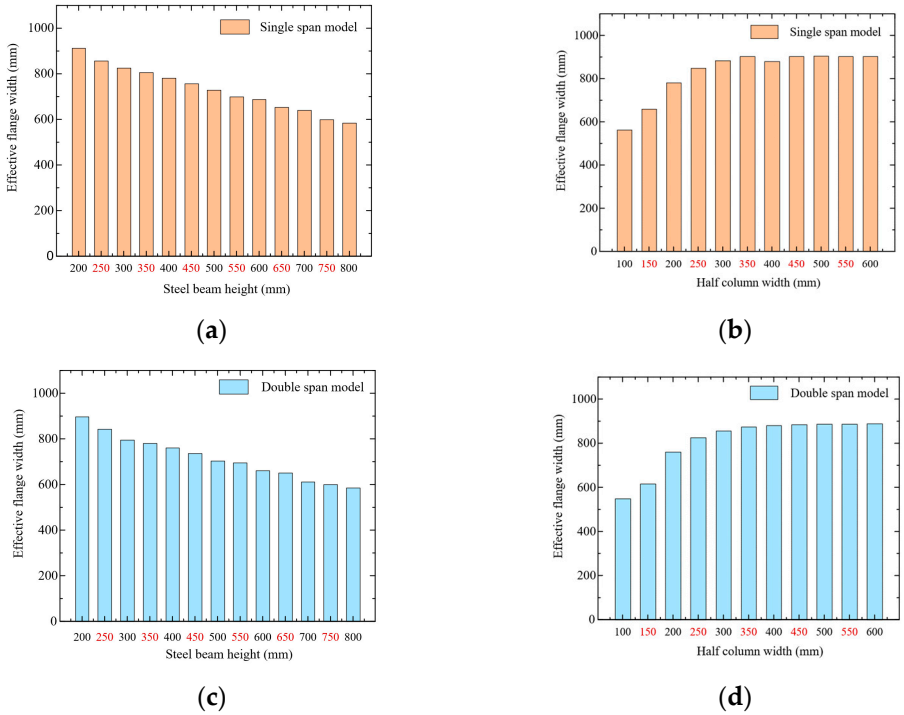

Figure 6. Influential parameters for side-column EFW. (**a**) EFWs for different steel-beam heights in the single-span model. (**b**) EFWs for different column widths in the single-span model. (**c**) EFWs for different steel-beam heights in the double-span model. (**d**) EFWs for different column widths in the single-span model.

3.2.2. Single-Span and Double-Span Models

The single-span model can be used only on the EFWs of HMRs in the side column, whereas the double-span model can reflect the EFWs of both the side and centre columns. Figure 6 shows that the EFW of the side column in the double-span model is close to that in the single-span model, mainly affected by the CFST half-width (R) and steel-beam height (h_s). Therefore, the EFW of the HMR for the centre and side columns is studied together under the uniform-loading condition of the double-span models. Differences between the influential parameters can then be obtained via comparison.

3.2.3. Influencing-Principle Analysis

As shown in Figure 7, when R is less than 300 mm, the stress curve expands outwards, such that the area around the curve increases as R increases. When this area increases, the EFW is enhanced. However, when R is greater than 300 mm, the growth of the area along with R is limited by the unchanging steel beam flange, as shown in Figure 8. The stress area remains almost unchanged, and the EFW does not change. With regard to the influential parameter h_s, the bending section is composed of steel beams and slab reinforcement layers. As h_s is increased, the sectional moment of inertia increases. When the distance between the slab reinforcement layer and the neutral axis is changed slightly, the overall stress values of the reinforcement decrease, and thus, the EFW of the HMR decreases. Finally, R and h_s can be utilised as two linearly related parameters to derive a formula for calculating the EFW of the side column, which will be presented later.

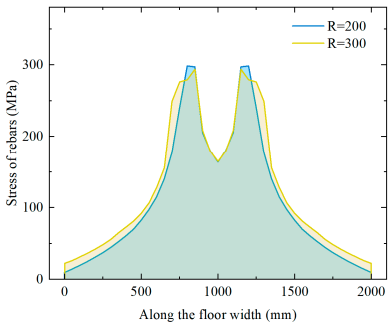

Figure 7. Stress distribution along slab width (R < 300 mm).

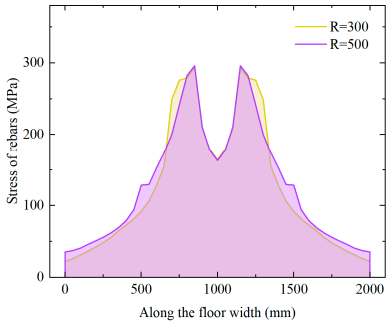

Figure 8. Stress distribution along slab width ($R \geq 300$ mm).

3.2.4. Irrelevant Parameters for Side Columns

In addition to the two parameters R and h_s mentioned earlier, other parameters have a certain impact on the EFW. However, the changes they produce are less than 15% relative to the reference model, and thus, these parameters are not used as key factors and are considered irrelevant. Plotting the EFWs for different CFST geometric parameters, as shown in Figure 9, reveals that H and t_{co} have little effect on the reinforcement stress results. Similarly, Figure 10 shows that bf_{btoom}, t_f, and t_w are irrelevant to the EFW, exhibiting no covariation. Although bf_{top} has some effect when it is equal to the column-tube width (400 mm), the variation has not exceeded 115% of the standard EFW (760 mm) and does not account for influential parameters. All five parameters listed in Figure 11 have little relation to the EFWs of the side columns, which is significantly different from the findings for the ultimate limit state [13]. When b_c increases, EFW does not change, whereas l changes the stress by changing the moment in the HMR but does not lead to variations exceeding 15%, as shown in Figure 12.

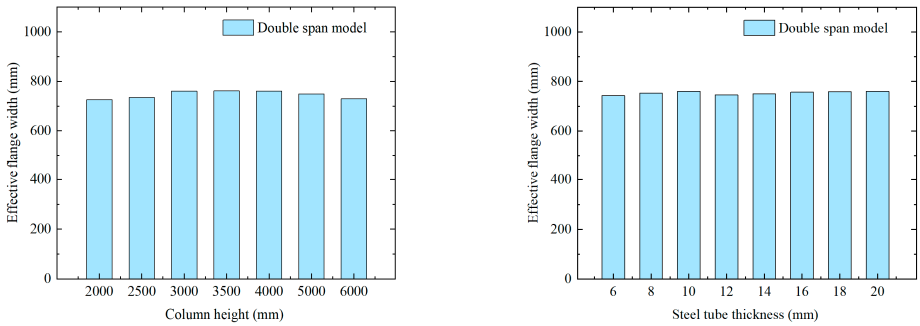

Figure 9. Irrelevant column parameters for side-column EFW. (**a**) EFWs for different column heights in the double-span model. (**b**) EFWs for different steel-tube thicknesses in the double-span model.

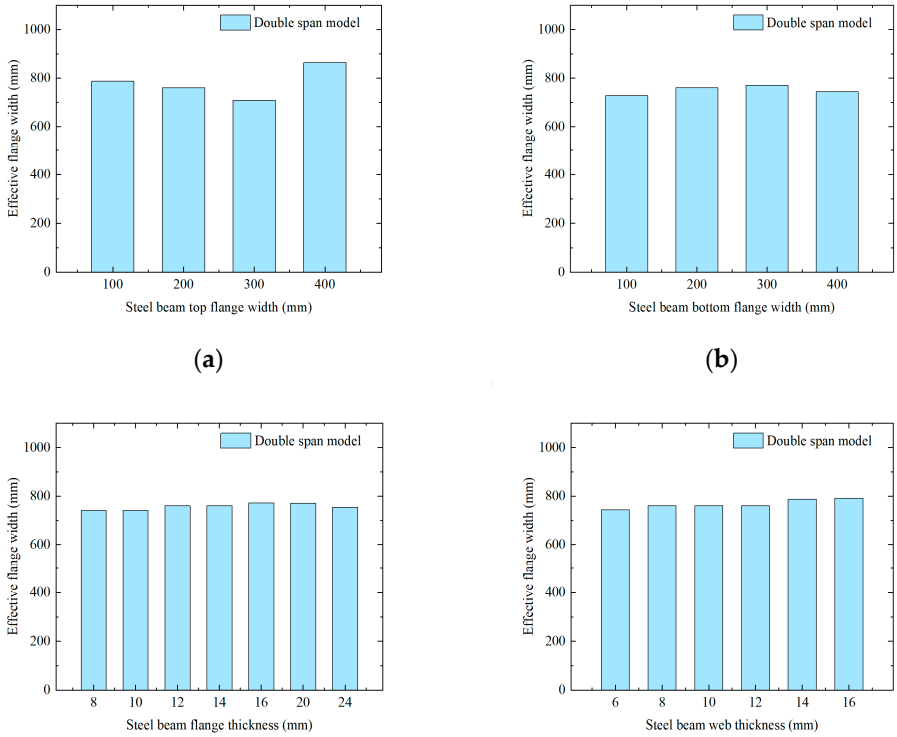

Figure 10. Irrelevant steel-beam parameters for side-column EFW. (**a**) EFWs for different steel-beam top-flange widths in the double-span model. (**b**) EFWs for different steel-beam bottom-flange widths in the double-span model. (**c**) EFWs for different steel-beam flange thicknesses in the double-span model. (**d**) EFWs for different steel-beam web thicknesses in the double-span model.

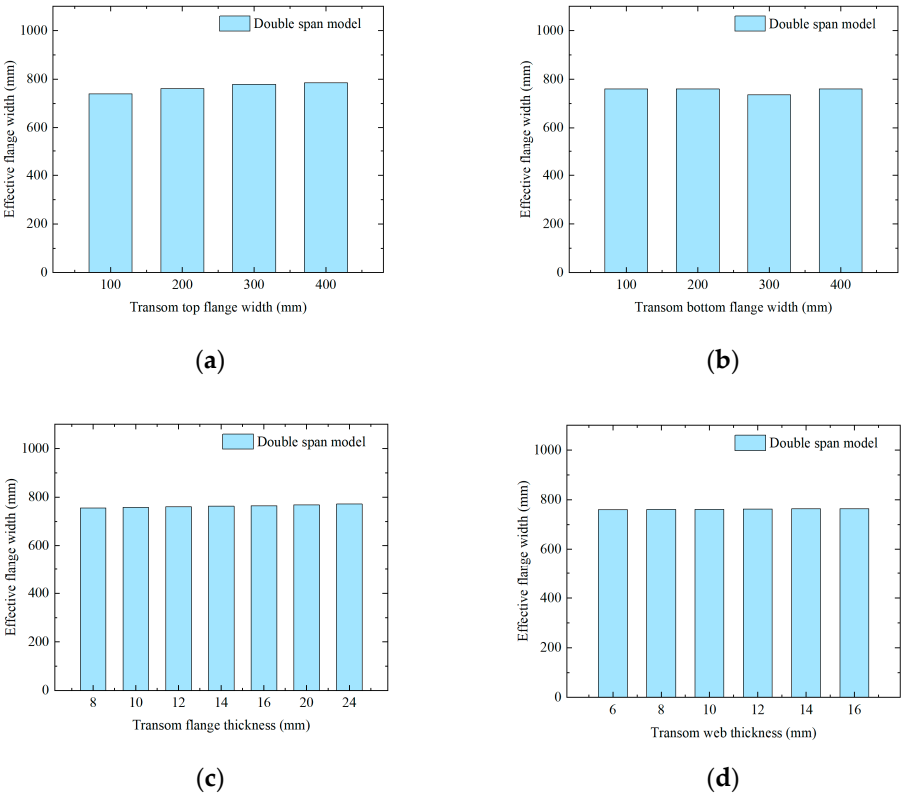

Figure 11. *Cont*.

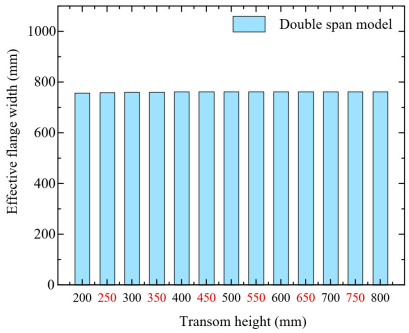

(**e**)

Figure 11. Irrelevant transom parameters for side-column EFW. (**a**) EFWs for different transom top-flange widths in the double-span model. (**b**) EFWs for different transom bottom-flange widths in the double-span model. (**c**) EFWs for different transom flange thicknesses in the double-span model. (**d**) EFWs for different transom web thicknesses in the double-span model. (**e**) EFW for different transom heights in the double-span model.

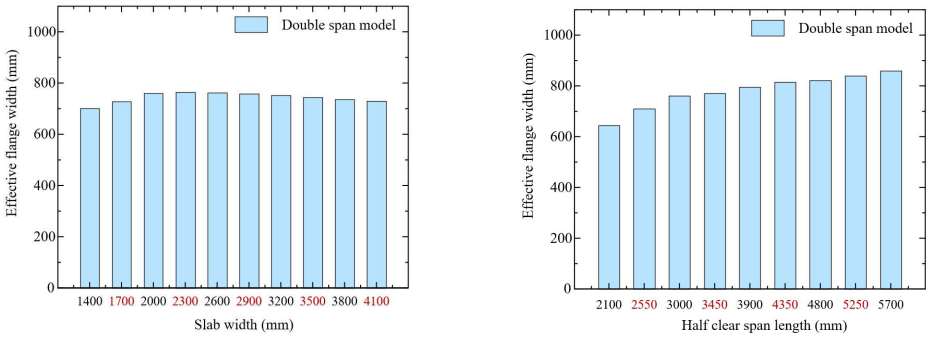

(**a**) (**b**)

Figure 12. Irrelevant slab parameters for side-column EFW. (**a**) EFWs for different slab widths in the double-span model. (**b**) EFWs for different clear-span lengths in the double-span model.

3.3. EFW of Centre Columns

3.3.1. Influential Parameters for Centre Columns

The parameters influencing the EFW of the centre column are the slab breadth (b_c), slab span (l), and steel beam height (h_s), as shown in Figure 13. Among them, b_c and l have similar influencing trends on the EFW, both of which exhibit positive correlations. On the other hand, the effect of the steel beam height is similar to that of the side column in that both are negatively correlated to the EFW. All these parameters are linearly correlated to the EFW to a certain extent.

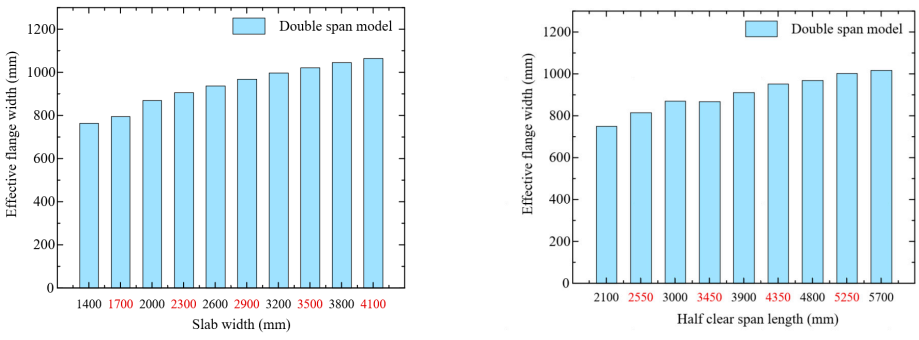

(**a**) (**b**)

Figure 13. *Cont.*

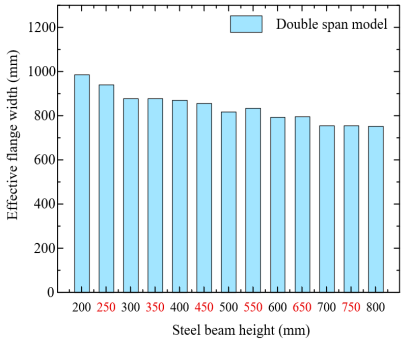

(**c**)

Figure 13. Influential parameters for centre-column EFW. (**a**) EFWs for different slab widths in the double-span model. (**b**) EFWs for different clear-span lengths in the double-span model. (**c**) EFWs for different steel-beam heights in the double-span model.

3.3.2. Influencing-Principle Analysis

According to the criteria for parameter sensitivity analysis, there are three influential parameters for the centre column, among which h_s presents a negative correlation with the EFW, which is consistent with the results for the side-column model; the influencing principle is that h_s increases the sectional moment of inertia and reduces the EFW. From the stress distributions of the centre and side columns along the width of the slab, as shown in Figure 14, it is evident that b_c will have different effects at the two positions. At the position of the centre column, the stress of the steel reinforcement outside the two peak points is between 35 and 50 MPa, in contrast to approximately 0 MPa in the side column. As b_c is increased, the area surrounding the stress curve increases significantly, and thus, the EFW also increases. Meanwhile, with regard to the effect of l on the EFW, the bending moment in the HMR increases as l is increased, which can also be reflected in the position of the side column. However, the resulting change exceeds 15%, and thus, l is regarded as an influential parameter in the analysis of the centre columns. Finally, b_c, l, and h_s can be utilised as three linearly related parameters to derive a formula for calculating the EFW of the centre column, which will be presented later.

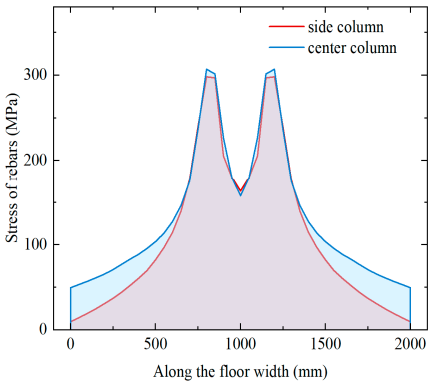

Figure 14. Stress distribution along slab width.

3.3.3. Irrelevant Parameters for Centre Columns

As shown in Figure 15, the irrelevant CFST parameters include H, h_s, and R. The effects of R differ significantly at the two locations. For the side column, R is positively correlated with the EFW until R reaches 300 mm. By contrast, for the centre column, R is negatively correlated with the EFW when R is less than 200 mm and then exhibits no further effect on the EFW after surpassing 200 mm. For the HMR of the centre column, the steel reinforcement generally has a tensile stress of 35–50 MPa, and the movement of the peak point has little influence on the surrounding area of the stress curve, showing to be

an irrelevant parameter after surpassing 200 mm. Although H slightly changes the EFW, it does not exceed the 15% threshold for changes due to a relevant parameter, and thus, H is not considered to be a critical factor. Figure 16 shows that the irrelevant geometric parameters of the steel beams are consistent with the insignificant effect exhibited by those of the side column. The transom parameters btr_{top}, btr_{bottom}, h_{tr}, t_{ftr}, and t_{wtr} are also all irrelevant parameters, as shown in Figure 17.

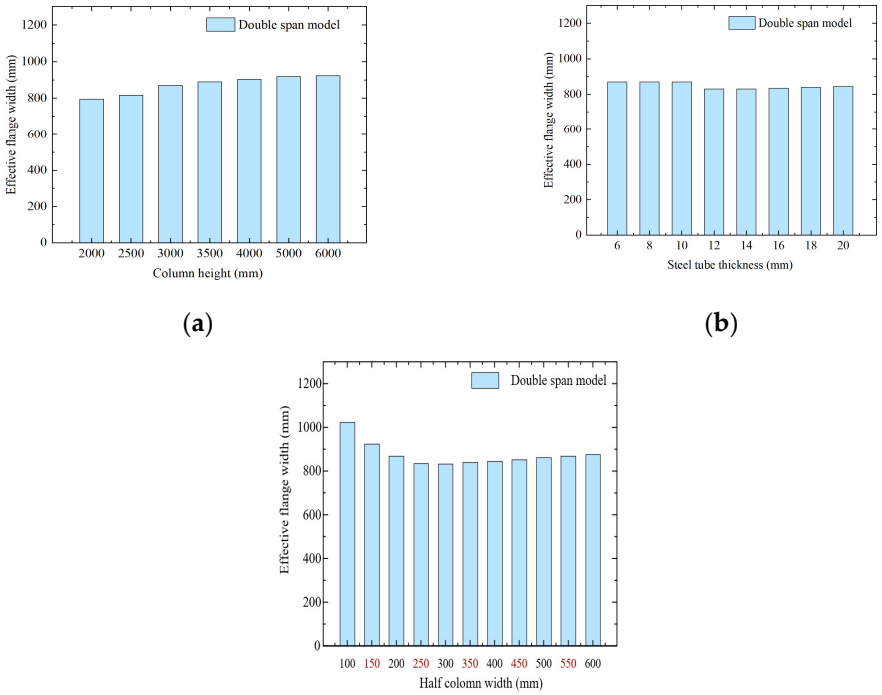

(**a**) (**b**)

(**c**)

Figure 15. Irrelevant column parameters for centre-column EFW. (**a**) EFWs for different column heights in the double-span model. (**b**) EFWs for different steel-tube thicknesses in the double-span model. (**c**) EFWs for different column widths in the double-span model.

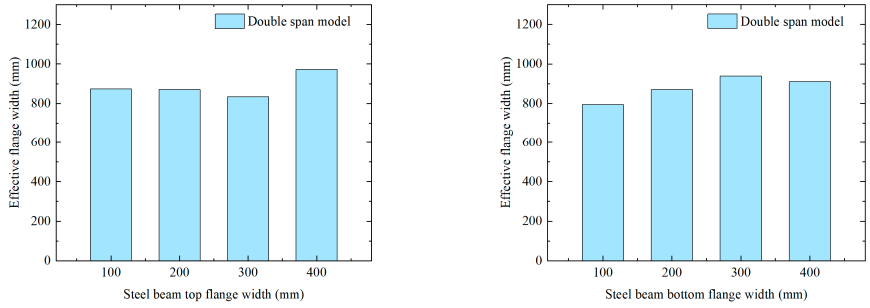

(**a**) (**b**)

Figure 16. *Cont.*

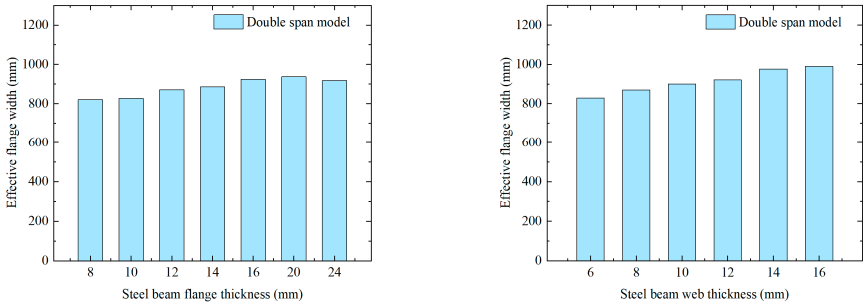

(**c**) (**d**)

Figure 16. Irrelevant steel-beam parameters for centre-column EFW. (**a**) EFWs for different steel-beam top-flange widths in the double-span model. (**b**) EFWs for different steel-beam bottom-flange widths in the double-span model. (**c**) EFWs for different steel-beam flange thicknesses in the double-span model. (**d**) EFWs for different steel-beam web thicknesses in the double-span model.

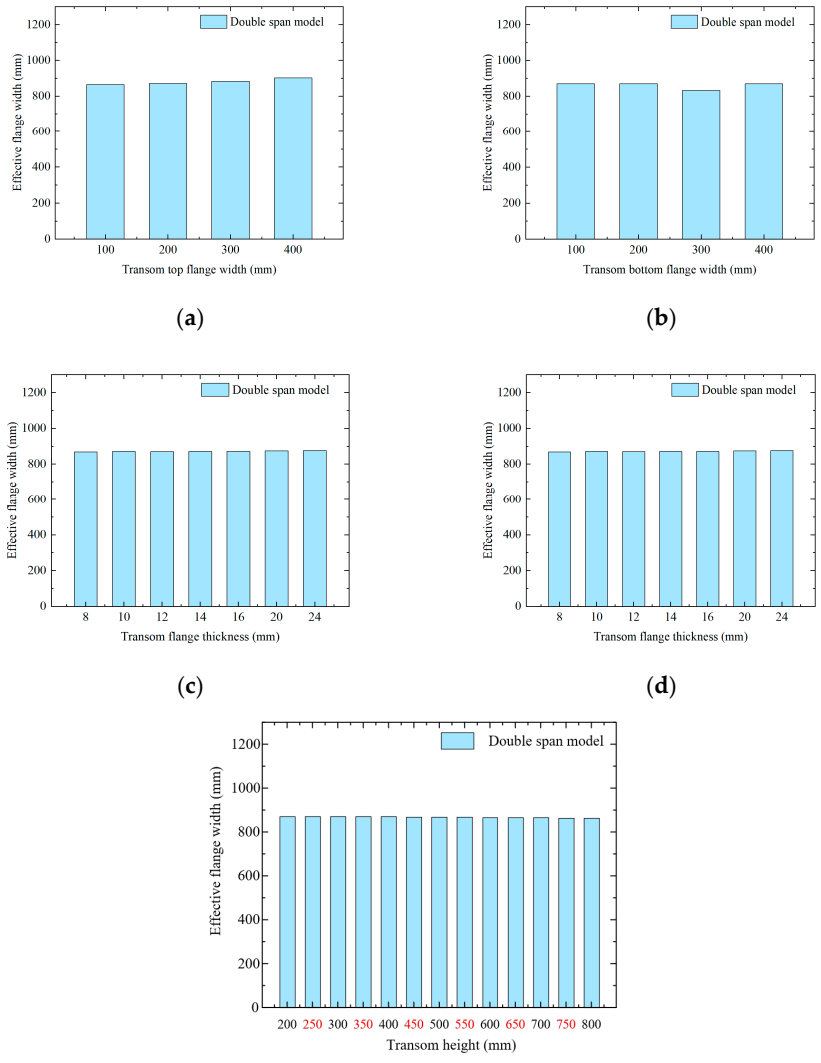

(**a**) (**b**)

(**c**) (**d**)

(**e**)

Figure 17. Irrelevant transom parameters for centre-column EFW. (**a**) EFWs for different transom top-flange widths in the double-span model. (**b**) EFWs for different transom bottom-flange widths in the double-span model. (**c**) EFWs for different transom flange thicknesses in the double-span model. (**d**) EFWs for different transom web thicknesses in the double-span model. (**e**) EFWs for different transom heights in the double-span model.

4. Effective Flange Width Formula: Derivation and Verification

An analysis of the stress distribution curve of the reinforcement under each parameter suggests that the maximum tensile stress of the reinforcement is always close to the yield strength. The material parameters are neither changed nor involved in the present study, and thus, based on Equation (3), the EFW is affected only by the area surrounding the stress curve. The EFW formulas for the side and centre columns of the double-span model are established according to the numerical relationship between the influential parameters and the EFW. Finally, the formulas are verified and discussed using a multiparameter model.

4.1. Effective Flange Width Formula for Side Columns

4.1.1. Fitting of Side-Column Design Formula

According to the results of the parameter sensitivity analysis, the parameters influential to the EFW of a side-column HMR are R and h_s. Under the influence of R, the EFW is distinctly segmented, and a linear relationship is maintained in each segment. Similarly, the EFW is also linearly affected by h_s. Thus, multiple linear regression was performed on the EFW as the dependent variable and R and h_s as the independent variables. The resulting regression formula is as follows:

$$b_e = \begin{cases} 1.358 \times R - 0.445 \times h_s + 653.091 & R \leq 300\text{mm} \\ 0.018 \times R - 0.445 \times h_s + 1054.864 & R > 300\text{mm} \end{cases} \quad (4)$$

The formula is divided into two parts by R = 300 mm, and the function values on both sides of the subsection point remain the same. The formula fitting of R and h_s are shown in Figure 18 and Figure 19, respectively.

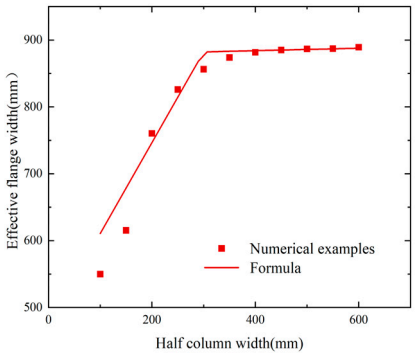

Figure 18. Numerical and proposed-formula results for half column width (R) in side columns.

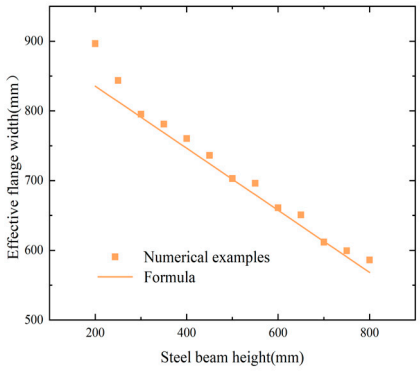

Figure 19. Numerical and proposed-formula results for steel-beam height (h_s) in side columns.

4.1.2. Formula Verification

Equation (4) was verified by establishing multiparameter variation models. To analyse the difference between the EFW calculated by the design formula (EFWD) and that calculated

by the new model (EFWM), the values of R and h_s were made to traverse their corresponding ranges outlined in Table 3; the resulting image is shown in Figure 20. The horizontal and vertical axes represent the EFWs calculated using the simulation models and the design formula, respectively. Based on the 143 two-parameter models obtained by varying R and h_s, and the 112 single-parameter models from Table 3, the difference between EFWD and EFWM is overwhelmingly less than 15%, indicating that the design formula produces a favourable prediction and can be used in engineering crack-checking calculations.

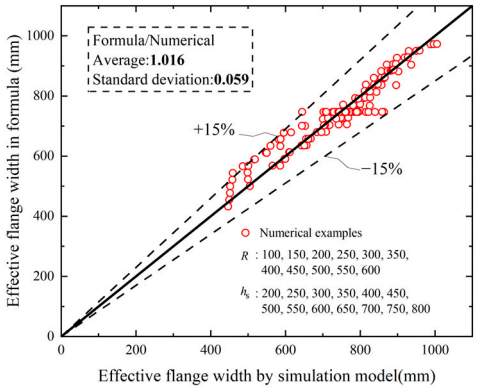

Figure 20. Ratio of EFWD to EFWM for side column.

4.2. Effective Flange Width Formula for Centre Columns

4.2.1. Fitting of Centre-Column Design Formula

In contrast to the HMR of the side column, the influential parameters of the centre column can be determined from the sensitivity analysis; in this case, the influential parameters are l, b_c, and h_s. The design formula in engineering needs to be kept as simple and convenient to use as possible; therefore, the influence of these three variables is also predicted using multiple linear regression. The proposed formula, segmented at l = 3000 mm, is as follows:

$$b_e = \begin{cases} 0.126 \times l + 0.104 \times b_c - 0.337 \times h_s + 417.065 & l \leq 3000\text{mm} \\ 0.057 \times l + 0.104 \times b_c - 0.337 \times h_s + 623.543 & l > 3000\text{mm} \end{cases} \quad (5)$$

In this context, b_e represents the EFW; l, b_c, and h_s represent the steel-beam height, slab width, and half clear-span length, respectively. The formula fitting of l, b_c, and h_s are shown in Figure 21, Figure 22, and Figure 23, respectively.

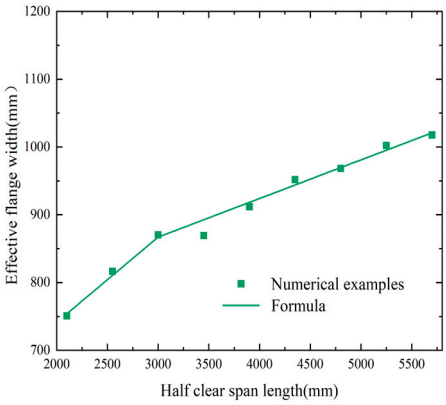

Figure 21. Numerical and proposed-formula results for half clear-span length (l) in center columns.

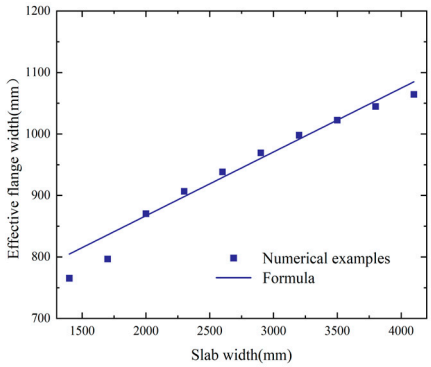

Figure 22. Numerical and proposed-formula results of slab breadth (b_c) in center columns.

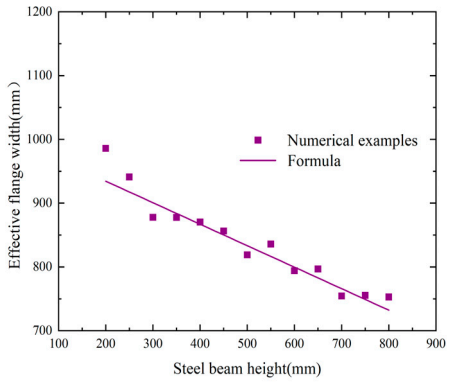

Figure 23. Numerical and proposed-formula results for steel-beam height (h_s) in center columns.

4.2.2. Formula Verification

Similarly, Equation (5) was also subjected to multiparameter variation model verification. To analyse the difference between EFWD and EFWM, the values of l, b_c, and h_s were made to traverse their corresponding ranges outlined in Table 3; the resulting image is shown in Figure 24.

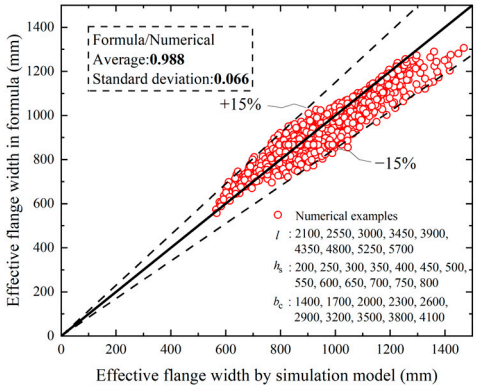

Figure 24. Ratio of EFWD to EFWM for centre column.

The horizontal and vertical axes represent the EFWD and EFWM, respectively. Based on the 1282 three-parameter models obtained by varying b_c, l, and h_s, and the 112 single-parameter models from Table 3, the difference between EFWD and EFWM is almost less than 15%. In some test samples, EFWD was higher than EFWM, mainly in models with small spans and large steel-beam heights. However, these parameters rarely appear in engineering constructions, and thus, these special parameter groups were removed from

Figure 24. Nonetheless, this design formula still produces a favourable prediction and can be used in engineering crack-checking calculations.

5. Comparison between Formulae

Specifications EC4 (Eurocode 4) and AISC (American Institute of Steel Construction) provide the calculation of the EFW for the HMR of a composite beam under the shear lag effect [29,30]. The calculation methods are similar in that they are related mainly to the clear span ($2l$), which is one of the influential parameters included in the proposed formula. However, this is quite different from the results of the sensitivity analysis performed in this study on the influential parameters because l at the side-column joint does not significantly affect EFW in SLS. Moreover, the influential parameters are not limited to l at the centre-column joint.

The calculation formulas provided by EC4 and AISC for the centre-column joints are subsequently shown, and the calculation results are compared with those of the formula proposed in this study for the setup shown in Figures 25 and 26. Clearly, these two specifications do not account for the parameters of the EFW in their entirety, and the EFW is designed to be calculated conservatively compared with the simulation results. By contrast, the formula proposed in this study is not conservative, the parameters considered are comprehensive, and the error in the calculation result is small.

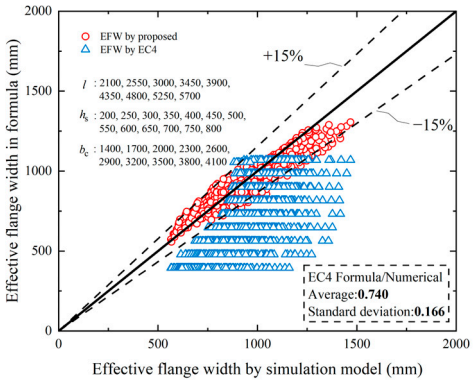

Figure 25. Comparison between EC4 and proposed formulae for centre columns.

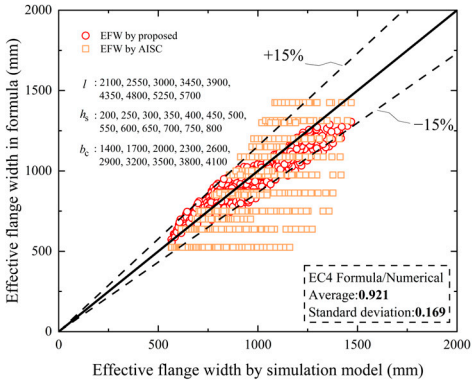

Figure 26. Comparison between AISC and proposed formulae for centre columns.

The formula from AISC for the EFW calculation is as follows:

$$\begin{gathered} b_e = \min\{b_0 + 2 \times \beta \times b_{fe}, 0.5 \times b_c\} \\ b_{fe} = 0.125 \times l \\ \beta = \min\left\{0.55 + 0.025 \times \frac{l}{b_{fe}}, 1\right\} \end{gathered} \quad (6)$$

where b_0 is equal to 0 for the composite beams of buildings, b_{fe} is the effective flange region of one side from the web, and β represents the reduction coefficient.

In this formula, l is still the major limiting factor:

$$b_e = \min\{0.25 \times l, 0.5 \times b_c\} \quad (7)$$

6. Conclusions

Through simulation and parameter analysis, the effective flange width of the HMR of a composite frame beam was investigated. The main conclusions of this study are summarised as follows:

(1) In the single-span and double-span CFB simulations, the simulation results for the side column were similar between the two models, and the difference in the EFW was less than 30 mm. Therefore, the double-span model can be used to simulate the stress on both the side and centre columns.

(2) In SLS of HMR, the maximum stress of some reinforcements can reach the yield strength; therefore, the EFW is affected only by the area surrounding the stress curve. From the parameter sensitivity analysis, it is evident that most geometric parameters, such as thickness, have little or no influence on the EFW.

(3) The parameters that affect the EFW of the side column include R and h_s. When R is less than or equal to 300 mm, there is a positive linear correlation with the EFW, whereas when R is greater than 300 mm, it has little effect on the EFW. On the other hand, h_s and EFW maintain a negative linear correlation. Based on the design formula using these two parameters as the independent variables, combined with their corresponding ranges of variation, the error between the predicted and simulated EFWs was determined to be less than 15%.

(4) The parameters that affect the EFW of the centre column include l, b_c, and h_s. The EFW is positively linearly correlated with b_c and l, and negatively linearly correlated with h_s, with segmentation at l = 3000 mm. The applicability of the formula was verified using combinations of the three parameters in varying ranges, and the error was found to be significantly less than 15%. Compared to those provided by EC4 and AISC, the calculation accuracy of the formulae proposed in this study improved significantly.

Finally, a formula for calculating the EFW for crack-width checking practice was proposed.

Future work that can be based on this study is to use similar modelling approaches to attempt the calculation of combined frame beams for applications in engineering practice. Also, the limitations of this study and the simplifying assumptions can be regarded as a direction for future exploration. In this study, the stress analysis is restricted to HMR, and the stress distribution of the sagging moment region in SLS remains to be analysed in the future. During the modelling process, the efficiency needs to be improved by some more convenient approaches. The slab thickness had been fixed to a constant value, excluded from the influential parameters, and the same assumption was made on material parameters.

Author Contributions: Conceptualisation, Z.-B.Z. and M.-X.T.; methodology, M.-X.T. and J.-Z.Z.; software, Z.-B.Z.; validation, Z.-B.Z.; formal analysis, M.-X.T.; investigation, Z.-B.Z. and J.-Z.Z.; resources, M.-X.T. and J.-Z.Z.; data curation, Z.-B.Z.; writing—original draft preparation, Z.-B.Z.; writing—review and editing, Z.-B.Z., M.-X.T. and J.-Z.Z.; visualisation, Z.-B.Z.; supervision, M.-X.T. and J.-Z.Z.; project administration, M.-X.T.; funding acquisition, M.-X.T. All authors have read and agreed to the published version of the manuscript.

Funding: The authors gratefully acknowledge the financial support provided by the National Natural Science Foundation of China (Grant No. 52178145).

Data Availability Statement: All data, models, and codes generated or used during the study are included in the submitted article.

Conflicts of Interest: The authors declare no conflicts of interest.

References

1. Nie, J.; Tao, M. Research and application of long-span steel-concrete spatial composite structures. *Spat. Struct.* **2009**, *15*, 17.
2. Nie, J.; Sun, T.; Wen, L.; Liu, J. Design of a long-span two-way steel-concrete composite beam floor system for a conference exhibition center. *J. Build. Struct.* **2004**, *25*, 123–125.
3. Nie, J.; Wei, J.; Chen, G. Application of composite steel-concrete beams in connecting structure between the buildings. *Build. Struct.* **2002**, *32*, 17–18.
4. He, L.; Maalla, A.; Zhou, X.; Tang, H. Buckling and post-buckling of anisogrid lattice-core sandwich plates with nanocomposite skins. *Thin Walled Struct.* **2024**, *199*, 111828. [CrossRef]
5. Huang, H.; Yao, Y.F.; Liang, C.J.; Ye, Y.X. Experimental study on cyclic performance of steel-hollow core partially encased composite spliced frame beam. *Soil Dyn. Earthq. Eng.* **2022**, *163*, 107499. [CrossRef]
6. Zhou, X.; Zhao, Y.; Liu, J.; Chen, Y.F.; Yang, Y. Bending experiment on a novel configuration of cold-formed U-shaped steel-concrete composite beams. *Eng. Struct.* **2019**, *180*, 124–133. [CrossRef]
7. Huang, H.; Huang, M.; Zhang, W.; Yang, S.L. Experimental study of predamaged columns strengthened by HPFL and BSP under combined load cases. *Struct. Infrastruct. Eng.* **2021**, *17*, 1210–1227. [CrossRef]
8. Qi, L.-K.; Li, L.; Chang, J.; Huo, D. Crack width in negative moment area of continuous steel-concrete composite beams. *J. Beijing Univ. Technol.* **2008**, *34*, 714–719. (In Chinese)
9. Du, X.; Luo, S.; Cheng, X.; Shi, H. Composite steel-concrete frame beam with reinforced negative bending regions. *J. Chongqing Jianzhu Univ.* **2006**, *28*, 56–58.
10. Elkelish, S.; Robinson, H. Effective widths of composite beams with ribbed metal deck. *Can. J. Civ. Eng.* **1986**, *13*, 575–582. [CrossRef]
11. Amadio, C.; Fragiacomo, M. Effective width evaluation for steel-concrete composite beams. *J. Constr. Steel Res.* **2002**, *58*, 373–388. [CrossRef]
12. Nie, J.G.; Tao, M.X. Slab spatial composite effect in composite frame systems. I: Effective width for ultimate loading capacity. *Eng. Struct.* **2012**, *38*, 171–184. [CrossRef]
13. Bursi, O.S.; Sun, F.-F.; Postal, S. Non-linear analysis of steel-concrete composite frames with full and partial shear connection subjected to seismic loads. *J. Constr. Steel Res.* **2005**, *61*, 67–92. [CrossRef]
14. Peng, W.; Tao, M. Study on effective flange width of end of composite frame beam with non-symmetrical steel section at ultimate limit state. *J. Build. Struct.* **2023**, *44*, 221–231. (In Chinese)
15. Peng, W.; Tao, M. Study on effective flange width of end of circular-section-column composite frame beam with non-symmetrical steel section at ultimate limit state. *Eng. Mech.* **2023**, *40*, 59–67, 256. (In Chinese)
16. Li, H.; Yang, Y.M.; Wang, X.Z.; Tang, H. Effects of the position and chloride-induced corrosion of strand on bonding behavior between the steel strand and concrete. *Structures* **2023**, *58*, 105500. [CrossRef]
17. Huang, M.S.; Wan, Z.H.; Cheng, X.H.; Xu, Z.A.; Lei, Y.Z.; Pan, D. Two-stage damage identification method based on fractal theory and whale optimization algorithm. *Adv. Struct. Eng.* **2022**, *25*, 2364–2381. [CrossRef]
18. Liu, Q.; Li, G.; Wang, J. A simplified method for side sway analyze of semi-rigid composite beam frame under serviceability limit states. *Chin. Q. Mech.* **2008**, *29*, 448–454. (In Chinese)
19. Nie, J.; Tao, M.; Cai, C.S.; Chen, G. Modeling and investigation of elasto-plastic behavior of steel-concrete composite frame systems. *J. Constr. Steel Res.* **2011**, *67*, 1973–1984. [CrossRef]
20. Wang, Y.H.; Nie, J.G. Effective flange width of steel-concrete composite beam with partial openings in concrete slab. *Mater. Struct.* **2015**, *48*, 3331–3342. [CrossRef]
21. Zhao, J.Z.; Zhou, Q.L.; Tao, M.X. Effective slab width for beam-end flexural strength of composite frames with circular-section columns. *J. Constr. Steel Res.* **2020**, *174*, 17. [CrossRef]
22. Tagawa, Y.; Kato, B.; Aoki, H. Behavior of composite beams in steel frame under hysteretic loading. *J. Struct. Eng.* **1989**, *115*, 2029–2045. [CrossRef]
23. Rüsch, H. Researches toward a general flexural theory for structural concrete. *ACI Struct. J.* **1960**, *57*, 1–28.
24. Huang, M.S.; Lei, Y.Z.; Li, X.F.; Gu, J.F. Damage Identification of Bridge Structures Considering Temperature Variations-Based SVM and MFO. *J. Aerosp. Eng.* **2021**, *34*, 04020113. [CrossRef]
25. Gluhović, N.; Marković, Z.; Spremić, M. Numerical parametric study on steel-concrete composite floor beams vibrations due to pedestrian traffic. *Građevinski Mater. I Konstr.* **2021**, *64*, 45–58. [CrossRef]
26. Huang, M.S.; Lei, Y.Z. Bearing Damage Detection of a Reinforced Concrete Plate Based on Sensitivity Analysis and Chaotic Moth-Flame-Invasive Weed Optimization. *Sensors* **2020**, *20*, 5488. [CrossRef]
27. Xu, L.-Y.; Tao, M.-X.; Zhou, M. Analytical model and design formulae of circular CFSTs under axial tension. *J. Constr. Steel Res.* **2017**, *133*, 214–230. [CrossRef]
28. Nie, J.; Tao, M. Deformation analysis of prestressing continuous steel-concrete composite beams. *China Civ. Eng. J.* **2007**, *40*, 38–45.

29. *ANSI/AISC 360-16*; Specification for Structural Steel Buildings. American Institute of Steel Construction: Chicago, IL, USA, 2016.
30. *BS EN 1994-1-1:2004*; Eurocode 4: Design of Composite Steel and Concrete Structures-Part 1-1: General Rules and Rules for Buildings. The British Standards Institution: London, UK, 2005.

Disclaimer/Publisher's Note: The statements, opinions and data contained in all publications are solely those of the individual author(s) and contributor(s) and not of MDPI and/or the editor(s). MDPI and/or the editor(s) disclaim responsibility for any injury to people or property resulting from any ideas, methods, instructions or products referred to in the content.